Nanomaterials

Lecture 17: Nanoscale Thermal Properties

Nanothermal Properties

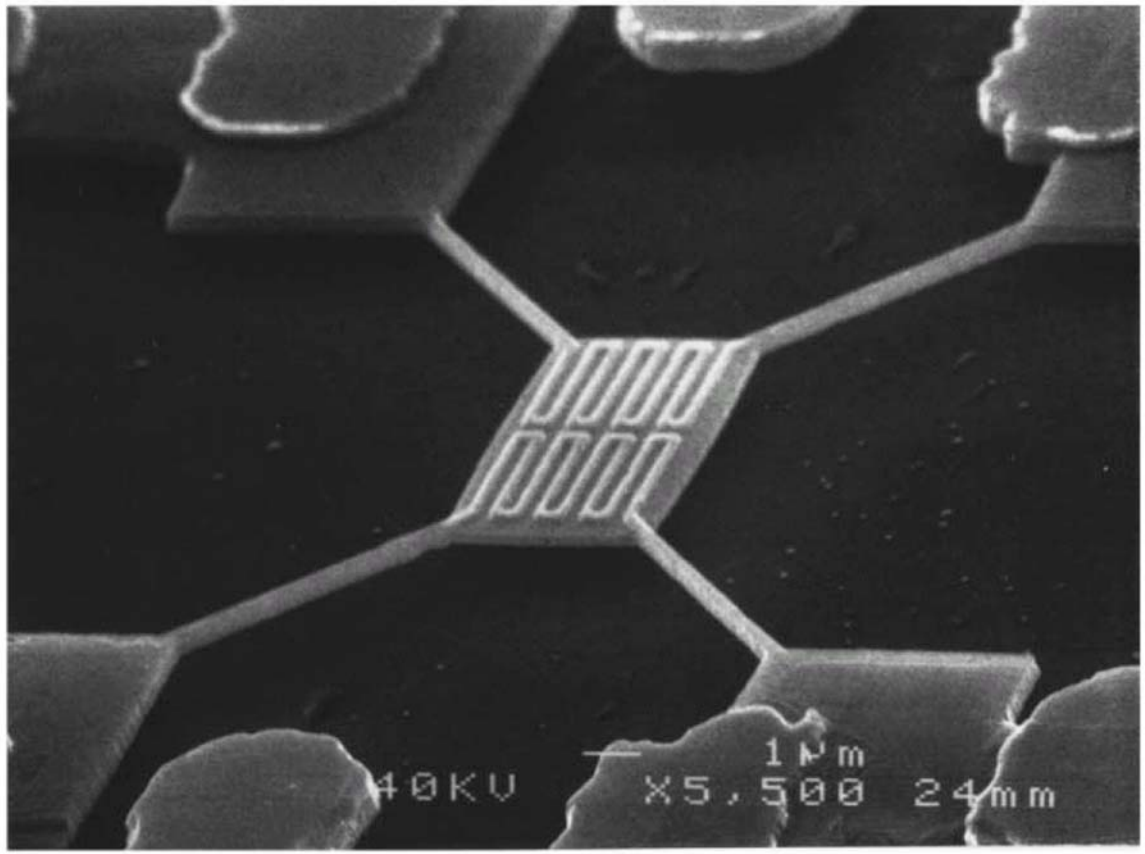

T.S. Tighe, *Appl. Phys. Lett.*, **70**, 2687 (1997).

Introduction to Thermoelectrics:
Seebeck Effect for Power Generation

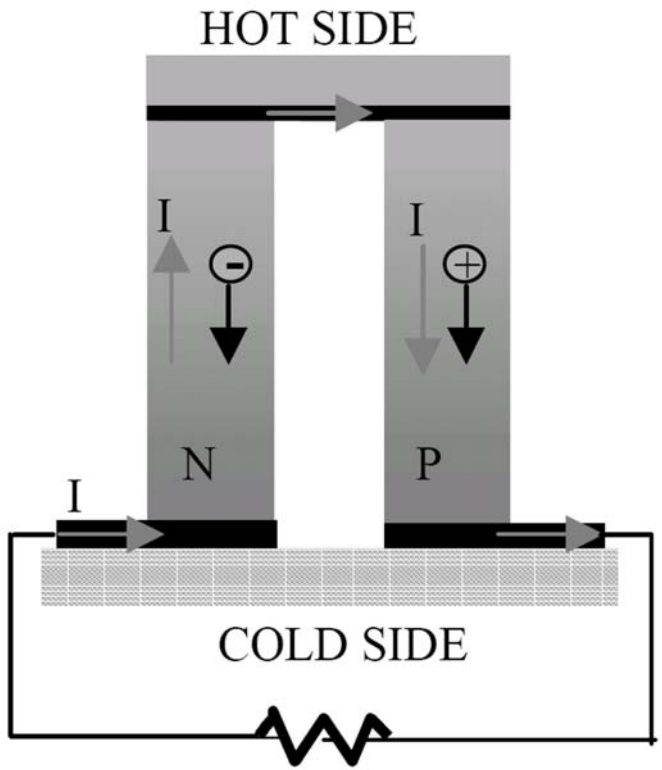

G. Chen, *et al.*, *Proc. Energy Conversion and Applications*, **1**, 28 (2001).

Introduction to Thermoelectrics:
Peltier Effect for Cooling

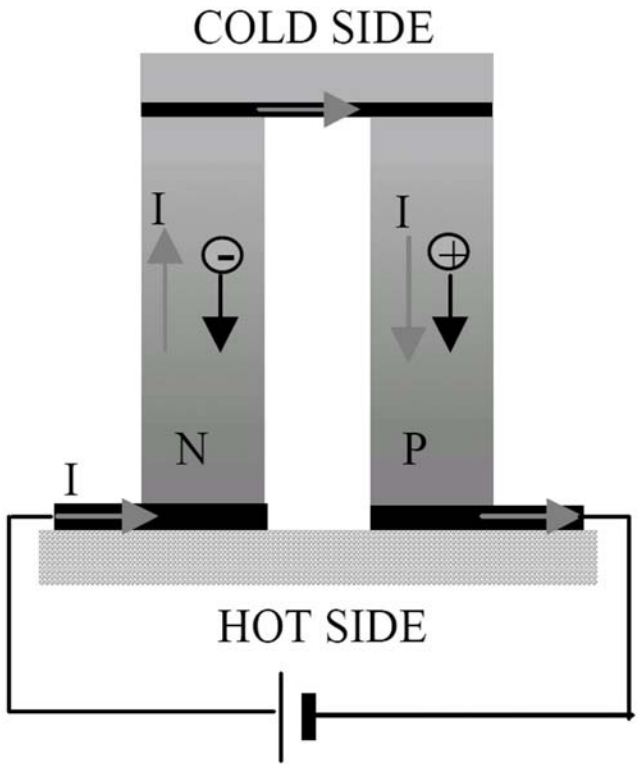

G. Chen, *et al.*, *Proc. Energy Conversion and Applications*, **1**, 28 (2001).

Example Thermoelectric Device

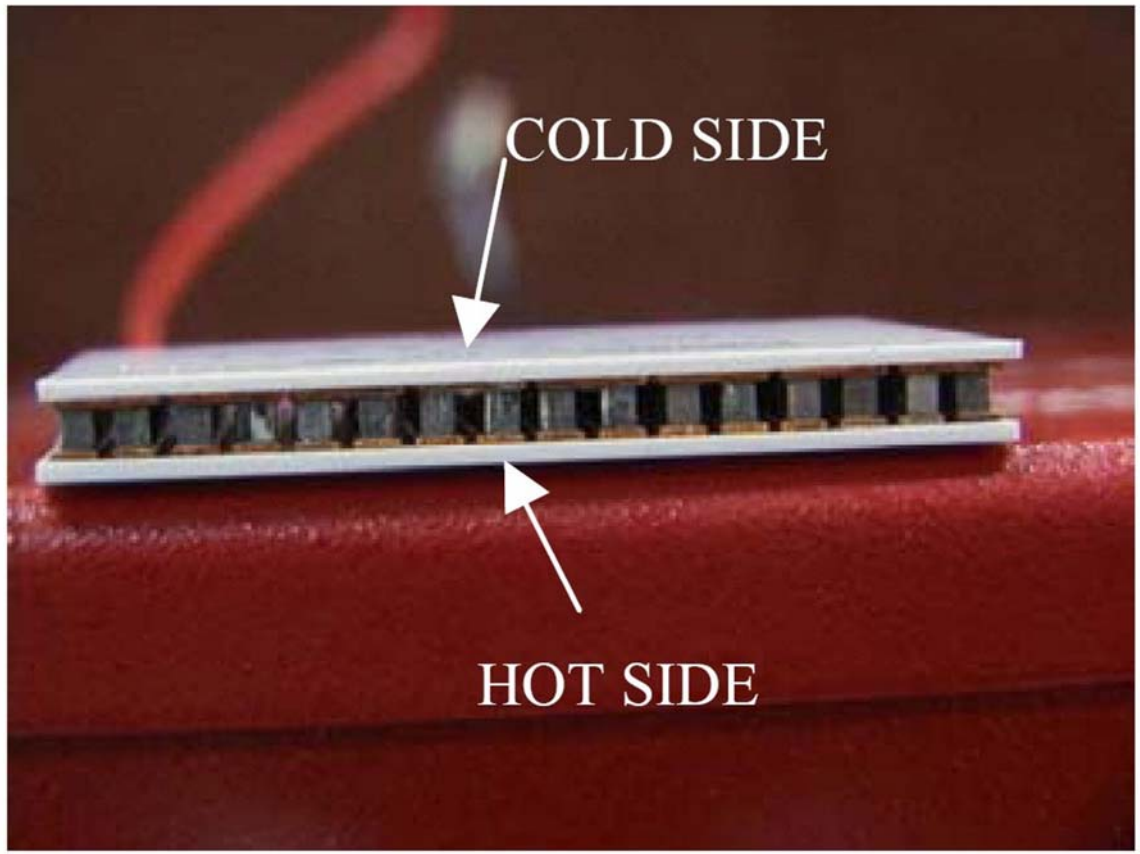

G. Chen, *et al.*, *Proc. Energy Conversion and Applications*, **1**, 28 (2001).

Efficiency of a Thermoelectric Device

Thermoelectric figure of merit:

$$Z = \frac{S^2 \sigma}{k}$$

S = Seebeck coefficient
(voltage generated per unit temperature between two points)

σ = electrical conductivity

k = thermal conductivity

Competitiveness of Thermoelectrics for Power Generation

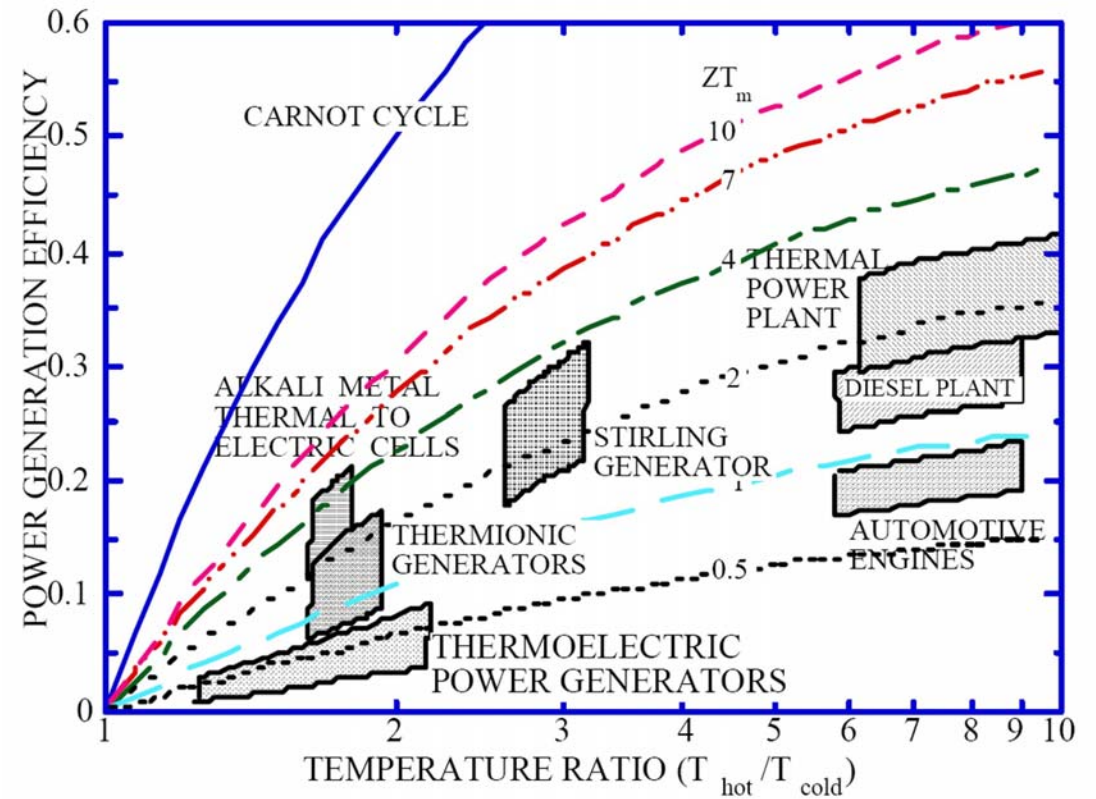

G. Chen, *et al.*, *Proc. Energy Conversion and Applications*, **1**, 28 (2001).

Competitiveness of Thermoelectrics for Cooling Applications

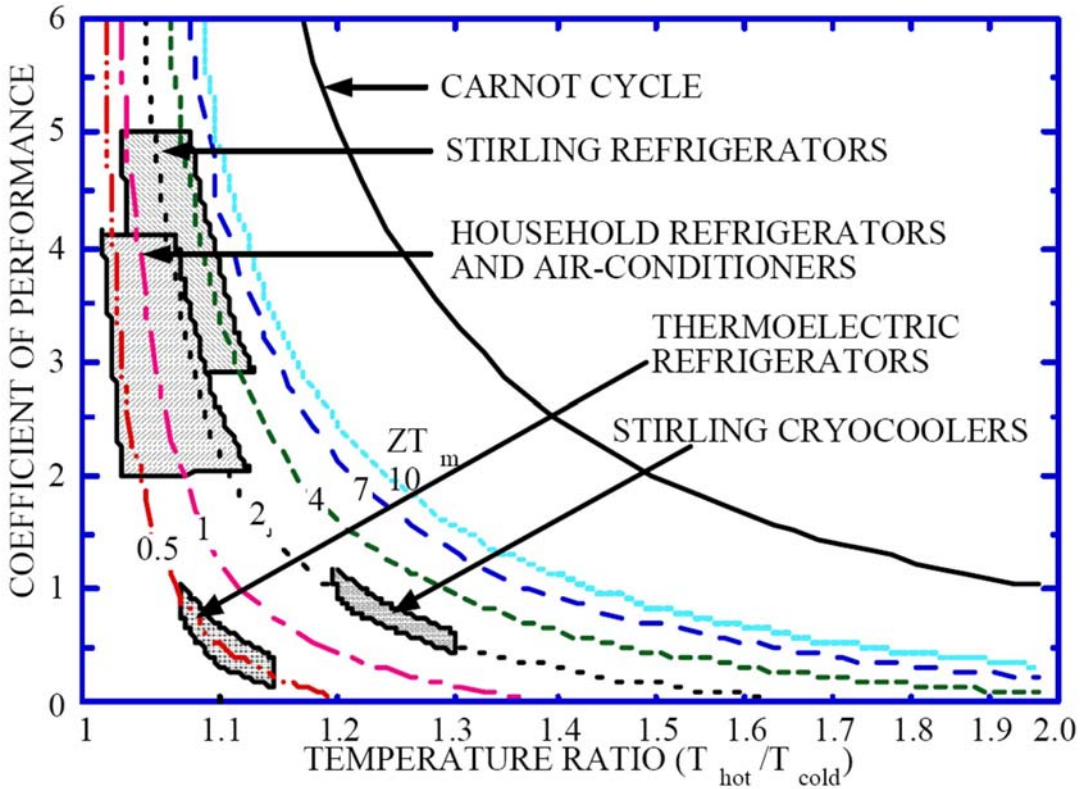

G. Chen, *et al.*, *Proc. Energy Conversion and Applications*, **1**, 28 (2001).

Improving Thermoelectric Figure of Merit

Thermoelectric figure of merit:

$$Z = \frac{S^2 \sigma}{k}$$

(1) Detailed analysis shows that Z is maximized when the average electron energy deviates from the Fermi energy → semiconductors

(2) To optimize σ, increase the number of free carriers

(3) To minimize k, increase phonon scattering

Enhancing the Density of States at the Nanoscale

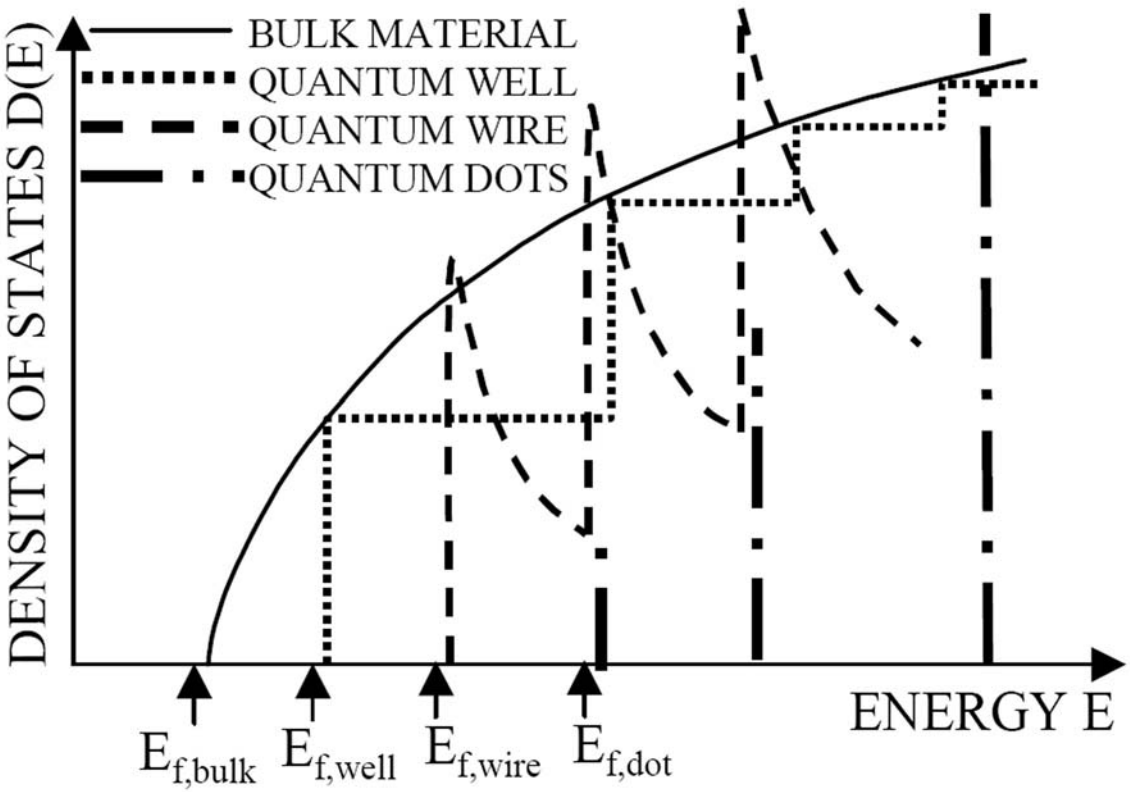

G. Chen, *et al.*, *Proc. Energy Conversion and Applications*, **1**, 28 (2001).

Enhancing Phonon Scattering with Heterostructures

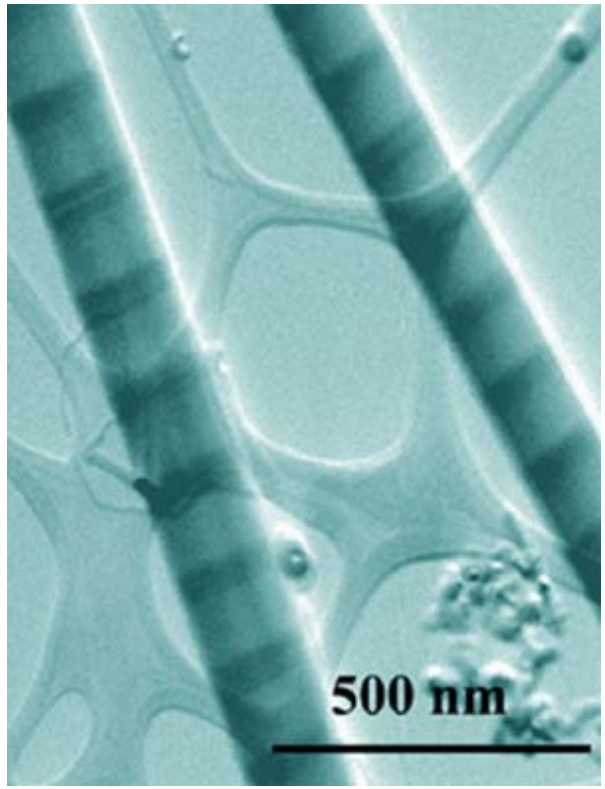

http://www.cchem.berkeley.edu/~pdygrp/images/gallery/

Example Thermoelectric Device

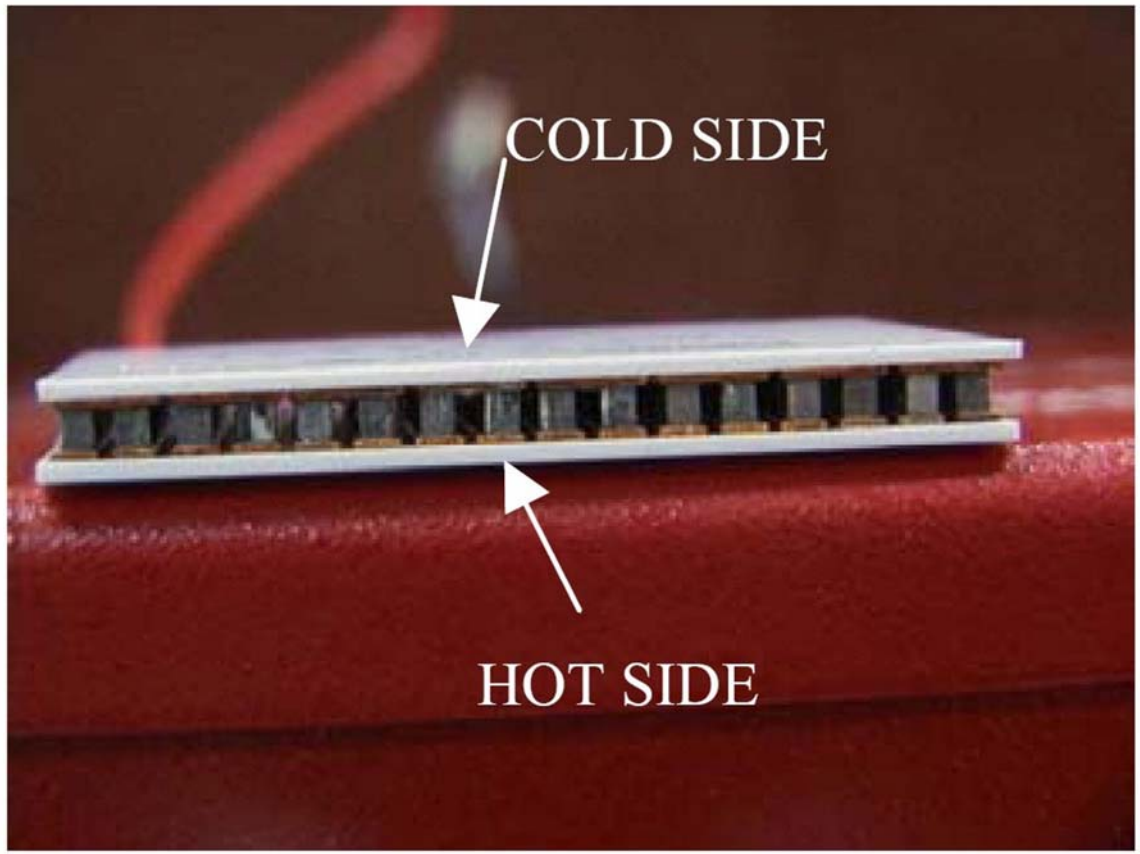

G. Chen, *et al.*, *Proc. Energy Conversion and Applications*, **1**, 28 (2001).

Exploring the Concept of Thermal Transport

In bulk materials, thermal transport is usually explained with two equations:

(1) Fourier's Law of Heat Conduction:

Heat flux: $\dot{Q} = -k\nabla T$

(2) Boltzmann Transport Equation (semi-classical model that treats electrons and phonons as classical particles – i.e., wave length nature is neglected).

D. G. Cahill, *et al.*, *J. Appl. Phys.*, **93**, 793 (2003).

Interface Effects

Thermal boundary resistance was first explored by Peter Kapitza in 1940 for the boundary between liquid helium and a solid.

The first model to explain this boundary resistance considered the acoustic mismatch at the boundary where the density and sound velocity discontinuously changes.

However, this simple model overestimated the boundary resistance by a factor of 10-100.

D. G. Cahill, *et al.*, *J. Appl. Phys.*, **93**, 793 (2003).

Importance of Defects at Surfaces and Interfaces

The discrepancy between theory and experiment was attributed to the existence of a compressed layer of helium at the surface of the solid.

This suggests that thermal transport across boundaries can be strongly influenced by surface defects.

These issues complicate the thermal transport analysis of many nanomaterials such as superlattices.

D. G. Cahill, *et al.*, *J. Appl. Phys.*, **93**, 793 (2003).

The Concept of Temperature

Temperature is typically defined as the average kinetic energy of a system of particles:

$$\left\langle \frac{1}{2} m_i v_i^{\,2} \right\rangle = \frac{3}{2} k_B T$$

However, quantum mechanically, the collective excitation of atomic motions are phonons whose average kinetic energy is given by:

$$\langle \frac{1}{2} m v_i^2 \rangle = \frac{1}{4N} \sum_{\lambda,\vec{q}} \hbar\omega_\lambda(\vec{q}) \xi^{(i)2}(\lambda,\vec{q}) \left[\frac{2}{e^{\hbar\omega_\lambda(q)/k_B T_i} - 1} + 1 \right]$$

D. G. Cahill, *et al.*, *J. Appl. Phys.*, **93**, 793 (2003).

The Concept of Temperature

In the limit of high temperature ($k_B T >> \hbar\omega_\lambda(q)$):

$$\frac{2}{e^{\hbar\omega_\lambda(q)/k_B T_i} - 1} + 1 \approx 2\frac{k_B T_i}{\hbar\omega_\lambda(\vec{q})}$$

In this limit, the quantum result and the classical result are the same.

However, for many materials, this limit is not valid (e.g., the optical phonons in silicon are 62 meV ~ 750 K).

D. G. Cahill, *et al.*, *J. Appl. Phys.*, **93**, 793 (2003).

2nd Lecture Begins

The Concept of Temperature

Temperature is typically defined as the average kinetic energy of a system of particles:

$$\left\langle \frac{1}{2} m_i v_i^{\,2} \right\rangle = \frac{3}{2} k_B T$$

However, quantum mechanically, the collective excitation of atomic motions are phonons whose average kinetic energy is given by:

$$\langle \frac{1}{2} m v_i^2 \rangle = \frac{1}{4N} \sum_{\lambda,\vec{q}} \hbar\omega_\lambda(\vec{q}) \xi^{(i)2}(\lambda,\vec{q}) \left[\frac{2}{e^{\hbar\omega_\lambda(q)/k_B T_i} - 1} + 1 \right]$$

D. G. Cahill, *et al.*, *J. Appl. Phys.*, **93**, 793 (2003).

The Concept of Temperature

In the limit of high temperature ($k_B T >> \hbar\omega_\lambda(q)$):

$$\frac{2}{e^{\hbar\omega_\lambda(q)/k_B T_i} - 1} + 1 \approx 2\frac{k_B T_i}{\hbar\omega_\lambda(\vec{q})}$$

In this limit, the quantum result and the classical result are the same.

However, for many materials, this limit is not valid (e.g., the optical phonons in silicon are 62 meV ~ 750 K).

D. G. Cahill, *et al.*, *J. Appl. Phys.*, **93**, 793 (2003).

The Concept of Temperature

Temperature is typically defined as the average kinetic energy of a system of particles:

$$\left\langle \frac{1}{2} m_i v_i^{\,2} \right\rangle = \frac{3}{2} k_B T$$

However, quantum mechanically, the collective excitation of atomic motions are phonons whose average kinetic energy is given by:

$$\langle \frac{1}{2} m v_i^2 \rangle = \frac{1}{4N} \sum_{\lambda,\vec{q}} \hbar\omega_\lambda(\vec{q}) \xi^{(i)2}(\lambda,\vec{q}) \left[\frac{2}{e^{\hbar\omega_\lambda(q)/k_B T_i} - 1} + 1 \right]$$

D. G. Cahill, *et al.*, *J. Appl. Phys.*, **93**, 793 (2003).

Implications for Fourier's Law

Although temperature can be defined for a single atom classically, the quantum mechanical definition can only be localized on the length scale of the phonon mean free path.

Since most of the heat is carried by phonons with large wave vectors, the relevant mean free paths are on the order of 1-100 nm.

Consequently, the notion of temperature is difficult to define in nanostructures, thus limiting the applicability of Fourier's Law of Heat Conduction.

D. G. Cahill, *et al.*, *J. Appl. Phys.*, **93**, 793 (2003).

Implications for the Boltzmann Transport Equation

Since the Boltzmann Transport Equation also relies a definition of local temperature, its applicability in nanostructures is limited.

Furthermore, the Boltzmann Transport Equation considers electrons and phonons classically, which neglects wave effects that are likely to become important in structures whose dimensions are comparable to the phonon mean free path and phonon wavelength.

D. G. Cahill, *et al.*, *J. Appl. Phys.*, **93**, 793 (2003).

Comparing Bulk to Thin Films

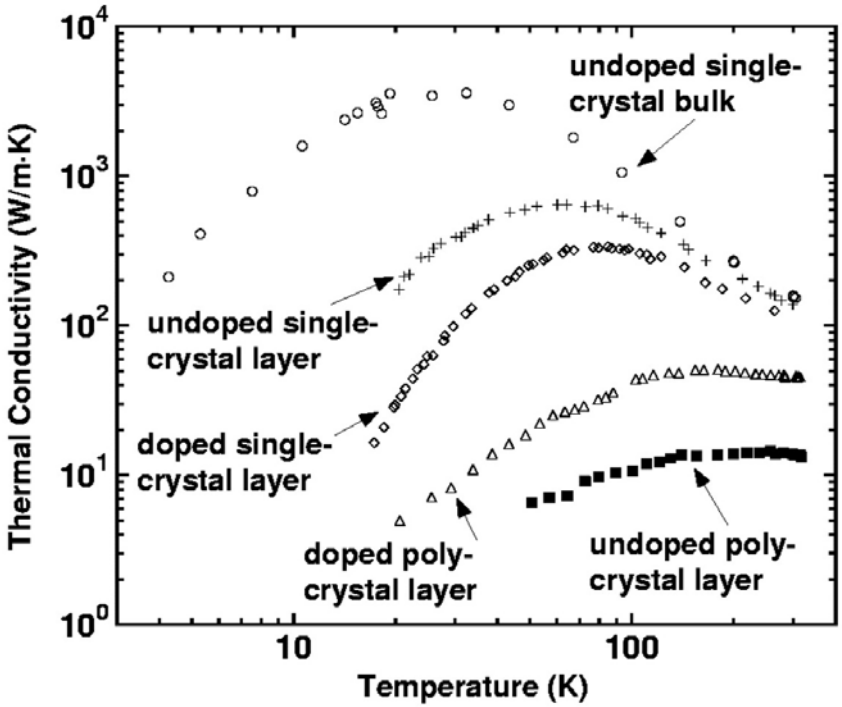

FIG. 5: Overview of thermal conductivity data for silicon films with varying microstructural quality and impurity concentrations after Ref. [58]. The data illustrate the relative importance of phonon scattering on film and grain boundaries and impurities. The data for undoped single-crystal bulk samples are taken from Ref. [59]. Both single crystal films have thickness of 3μm, and for the doped film, a boron concentration of 10^{19} cm^{-3} [55]. The undoped and doped (1.6×10^{19} cm^{-3} boron) polycrystalline films have grain sizes of 200 and 350 nm, respectively [57, 58].

D. G. Cahill, *et al.*, *J. Appl. Phys.*, **93**, 793 (2003).

Measuring Thermal Properties of Nanotubes

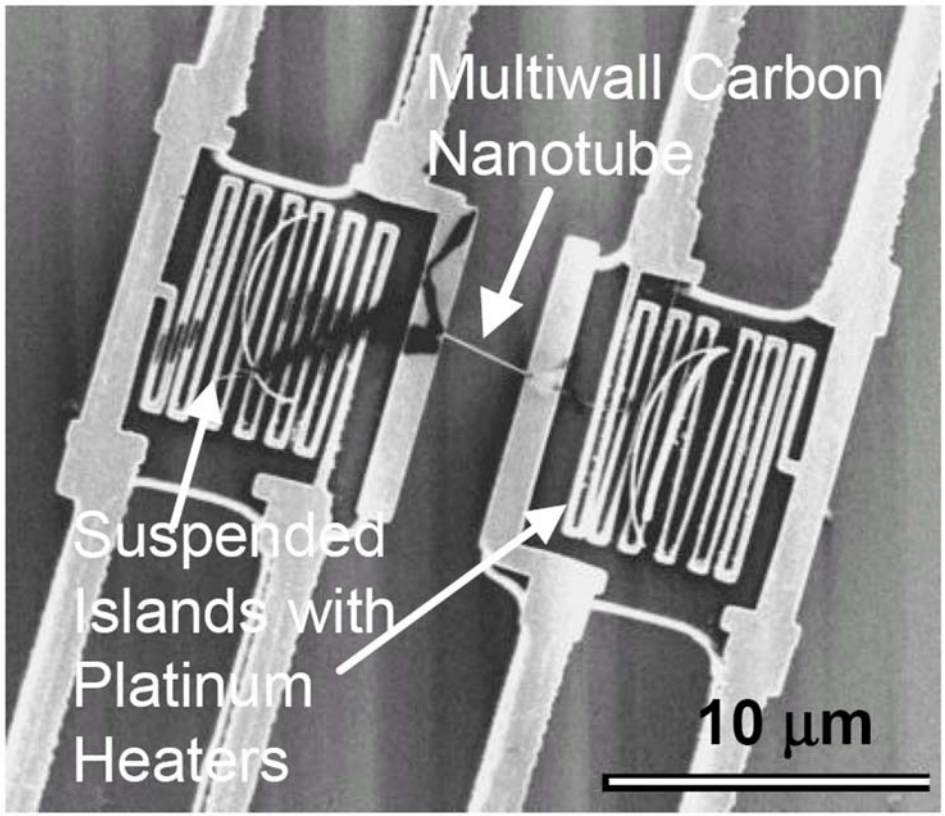

D. G. Cahill, *et al.*, *J. Appl. Phys.*, **93**, 793 (2003).

Scanning Thermal Microscope

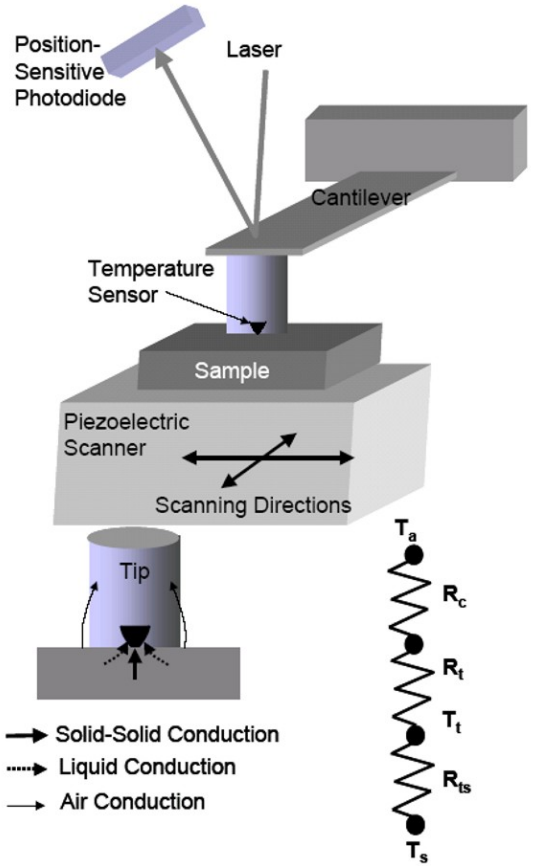

FIG. 17: Schematic diagram of a scanning thermal microscope (SThM). It consists of a sharp temperature-sensing tip mounted on a cantilever probe. The sample is scanned in the lateral directions while the cantilever deflections are monitored using a laser beam-deflection technique. Topographical and thermal images can be thermally obtained. The thermal transport at the tip-sample contacts consists of air, liquid and solid-solid conduction pathways. A simple thermal resistance network model of the sample and probe combination, shows that when the sample is at temperature T_s, the tip temperature T_t depends on the values of the thermal resistances of the tip-sample contact, R_{ts}, the tip, R_t, and the cantilever probe, R_c.

D. G. Cahill, *et al.*, *J. Appl. Phys.*, **93**, 793 (2003).

Scanning Thermal Microscopy of MWNTs

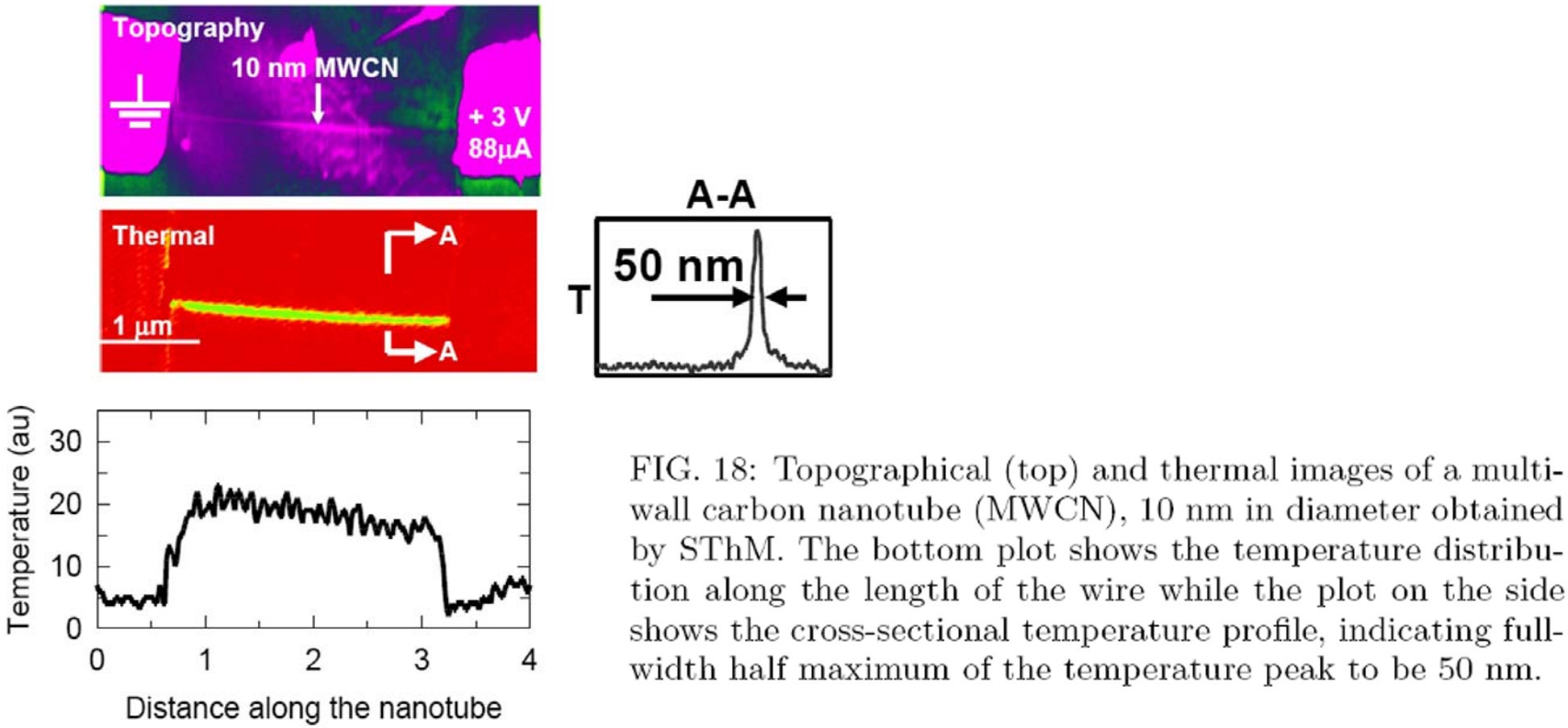

FIG. 18: Topographical (top) and thermal images of a multi-wall carbon nanotube (MWCN), 10 nm in diameter obtained by SThM. The bottom plot shows the temperature distribution along the length of the wire while the plot on the side shows the cross-sectional temperature profile, indicating full-width half maximum of the temperature peak to be 50 nm.

D. G. Cahill, *et al.*, *J. Appl. Phys.*, **93**, 793 (2003).

Phonon Transport in 1-D Nanostructures

In 3-D materials, phonons possess three polarizations: two transverse and one longitudinal.

In perfect 1-D materials, only one longitudinal polarization should be possible.

However, real 1-D materials possess surfaces which give rise to additional surface phonon modes.

The resulting change in the dispersion relation modifies the group velocity and density of states.

D. G. Cahill, *et al.*, *J. Appl. Phys.*, **93**, 793 (2003).

Phonon Lifetimes in 1-D Nanostructures

Phonon-phonon interactions change since energy conservation and wave-vector relations depend on the dispersion relation.

Furthermore, phonon boundary scattering is likely to be much more significant in 1-D nanostructures than 3-D materials.

The role of defects and coupling to electronic modes may also be significantly enhanced in 1-D nanostructures.

D. G. Cahill, *et al.*, *J. Appl. Phys.*, **93**, 793 (2003).

Measuring the Thermal Conductivity of Silicon Nanowires

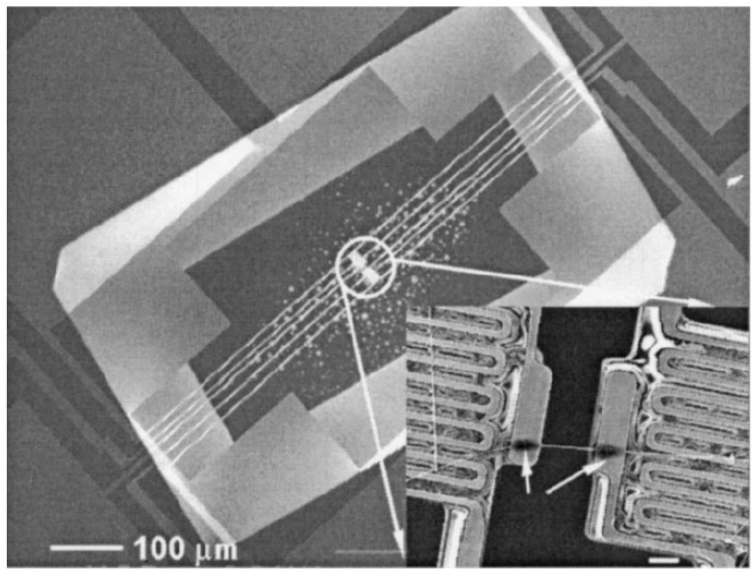

Pt wires serve as resistive heaters and resistance thermometers

FIG. 1. SEM image of the suspended heater. The lower inset shows a 100 nm Si nanowire bridging the two heater pads, with wire-pad junctions wrapped with amorphous carbon deposits (shown by arrows). The scale bar in the inset represents 2 μm.

D. Li, *et al.*, *Appl. Phys. Lett.*, **83**, 2934 (2003).

Thermal Conductivity Data for Silicon Nanowires

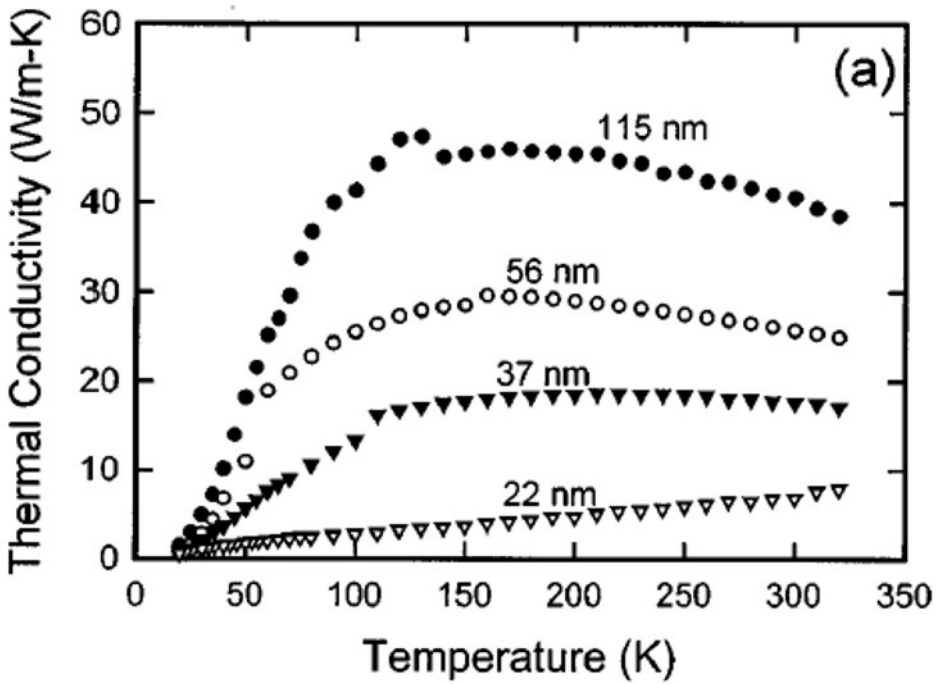

For all diameters, the thermal conductivity of silicon nanowires is approximately two orders of magnitude lower than the bulk.

D. Li, *et al.*, *Appl. Phys. Lett.*, **83**, 2934 (2003).

Thermal Conductivity Data for Silicon Nanowires

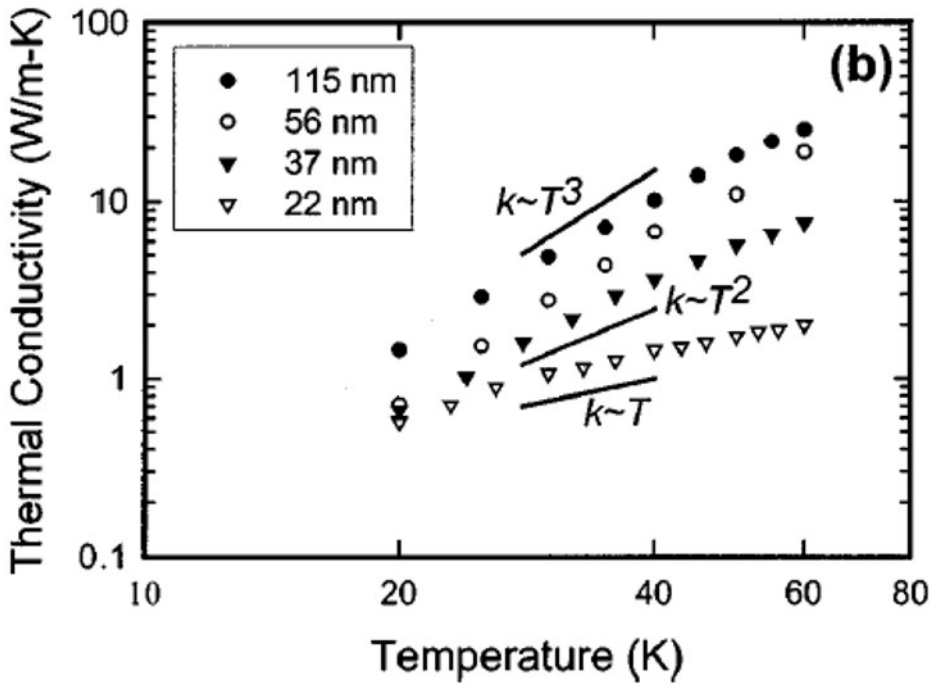

For small diameters, the data appears to deviate from the Debye T^3 law for specific heat.

D. Li, *et al.*, *Appl. Phys. Lett.*, **83**, 2934 (2003).

Measuring Thermal Conductivity for Si/SiGe Nanowires

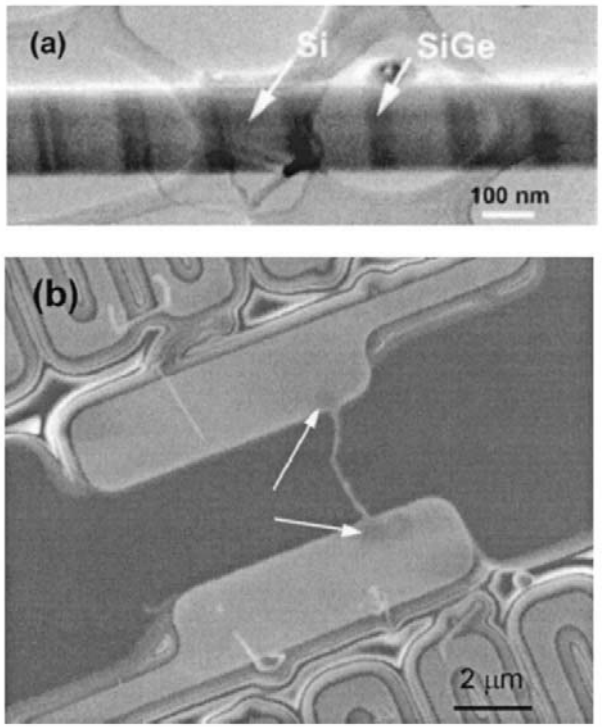

FIG. 1. (a) A transmission electron micrograph of a Si/SiGe superlattice nanowire. (b) A scanning electron micrograph of an 83 nm Si/SiGe superlattice nanowire bridging the two suspended heater pads. The arrows point to the carbon deposits.

D. Li, *et al.*, *Appl. Phys. Lett.*, **83**, 3186 (2003).

Thermal Conductivity Data for Si/SiGe Nanowires

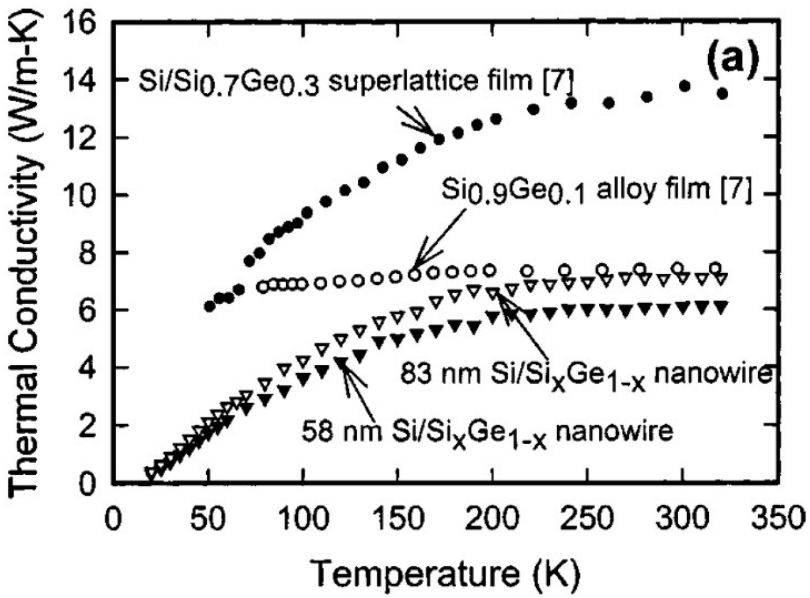

FIG. 2. (a) Thermal conductivities of 58 and 83 nm diameter single crystalline Si/Si_xGe_{1-x} superlattice nanowires. The value of x is $\sim 0.9-0.95$ and the superlattice period is 100–150 nm. Thermal conductivities of a 30 nm period 2D $Si/Si_{0.7}Ge_{0.3}$ superlattice film and $Si_{0.9}Ge_{0.1}$ alloy film (3.5 μm thick) are also shown. (b) Thermal conductivities of single crystalline pure Si nanowires. The number besides each curve denotes the corresponding wire diameter.

D. Li, *et al.*, *Appl. Phys. Lett.*, **83**, 3186 (2003).

Thermal Conductivity Data for Si/SiGe Nanowires

Observations:

(1) At high temperature, the thermal conductivity of the nanowire superlattice matches a pure Si_xGe_{1-x} alloy.

→ Alloy scattering of phonons is dominant as expected since the heterostructure modulation of x is only 0.1 (this implies that the acoustic mismatch is small, which minimizes interface scattering).

D. Li, *et al.*, *Appl. Phys. Lett.*, **83**, 3186 (2003).

Thermal Conductivity Data for Si/SiGe Nanowires

Observations:

(2) The thermal conductivity of the nanowire superlattice is much lower than pure silicon nanowires.

→ This behavior is also consistent with alloy scattering of phonons which would not be present in the pure silicon nanowires.

D. Li, *et al.*, *Appl. Phys. Lett.*, **83**, 3186 (2003).

Thermal Conductivity Data for Si/SiGe Nanowires

Observations:

(3) The thermal conductivity of the nanowire superlattice decreases with decreasing nanowire diameter.

→ This observation suggests that boundary scattering of phonons is also playing a role. However, the diameter dependence is much weaker than pure silicon nanowires since this effect is competing with significant alloy scattering.

D. Li, *et al.*, *Appl. Phys. Lett.*, **83**, 3186 (2003).

Thermal Conductivity Data for Si/SiGe Nanowires

Comments on competing scattering mechanisms:

(1) The efficiency of phonon alloy scattering follows the fourth power of the ratio of the defect size to phonon wavelength → short wavelength phonons are most efficiently scattered by atomic scale defects in alloys.

(2) Meanwhile, long wavelength phonons are scattered by the nanowire boundaries.

D. Li, *et al.*, *Appl. Phys. Lett.*, **83**, 3186 (2003).

Thermal Conductivity Data for Si/SiGe Nanowires

Comments on competing scattering mechanisms:

(3) As temperature is decreased, the long wavelength phonons play an increasingly important role in thermal transport.

(4) Consequently, the discrepancy between the thermal conductivity of the heterostructure nanowire and the bulk alloy increases with decreasing temperature.

D. Li, *et al.*, *Appl. Phys. Lett.*, **83**, 3186 (2003).

Probing the Quantum Limit of Thermal Conductance

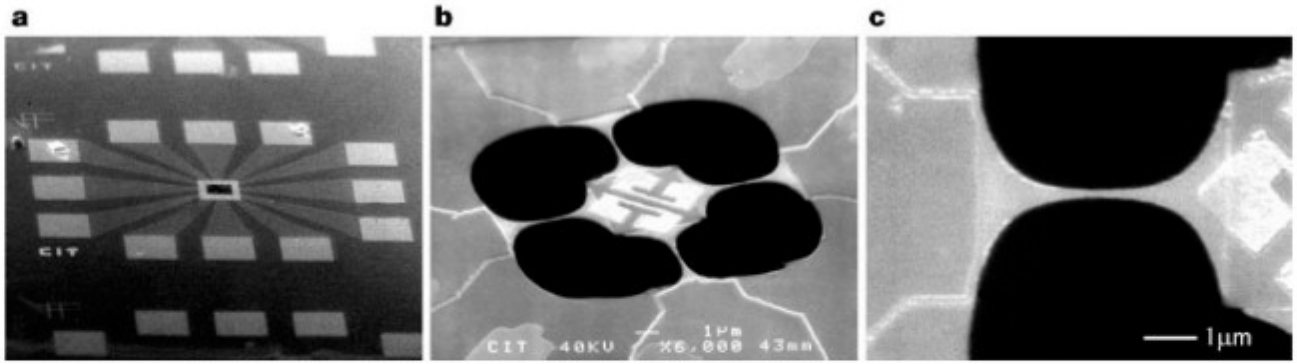

Figure 1 Suspended mesoscopic device. A series of progressive magnifications are shown. **a**, Overall view of the ~1.0 × 0.8 mm device, showing 12 wirebond pads that converge via thin-film niobium leads into the centre of the device. This central region is a 60-nm-thick silicon nitride membrane, which appears dark in the electron micrograph. **b**, View of the suspended device, which consists of a 4 × 4 μm 'phonon cavity' (centre) patterned from the membrane. In this view, the bright "c" shaped objects on the device are thin-film gold transducers, whereas in the dark regions the membrane has been completely removed. The transducers are connected to thin-film. niobium leads that run atop the 'phonon waveguides'; these leads ultimately terminate at the wirebond pads. **c**, Close-up of one of the catenoidal waveguides, displaying the narrowest region which necks down to <200-nm width.

K. Schwab, *et al.*, *Nature*, **404**, 974 (2000).

Probing the Quantum Limit of Thermal Conductance

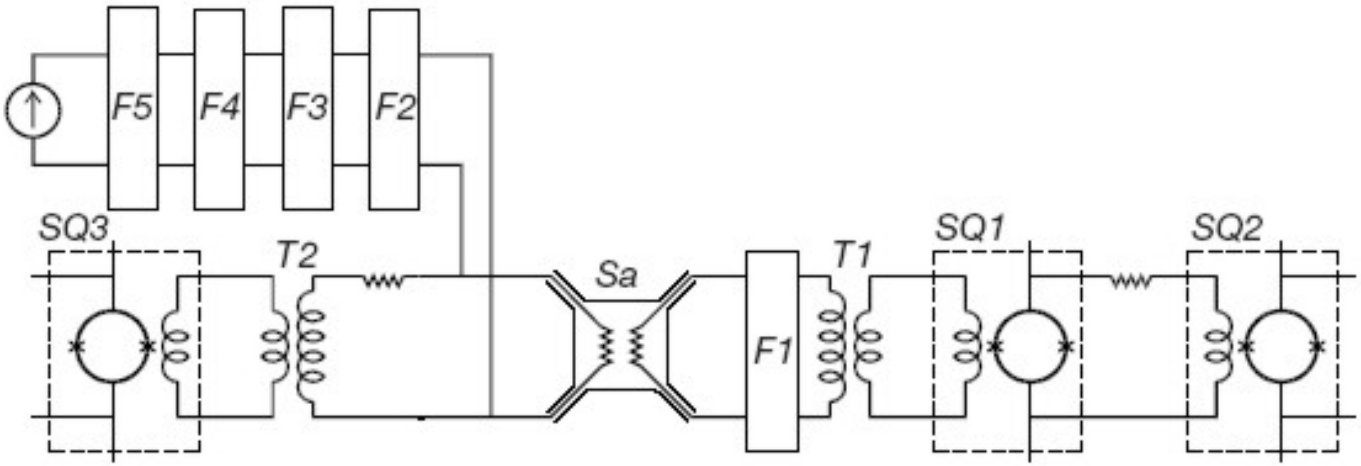

- Resistive gold heater/thermometer at the suspended sample.
- Sensing accomplished with a SQUID thermometry circuit.

K. Schwab, *et al.*, *Nature*, **404**, 974 (2000).

Thermal Conductance of Phonon Waveguides in the Ballistic One-Dimensional Limit

In the limit of linear response ($\Delta T \ll T$),

$$G_{\mathrm{th}} = \frac{J_{\mathrm{th}}}{\Delta T} = \frac{k_{\mathrm{B}}^2}{h} \sum_m \int_{x_m}^{\infty} \mathrm{d}x \frac{x^2 e^x}{(e^x - 1)^2} T_m(x k_{\mathrm{B}} T/\hbar)$$

where $T_m(\omega)$ is the transmission coefficient that characterizes the coupling of the waveguide modes to the reservoirs.

K. Schwab, *et al.*, *Nature*, **404**, 974 (2000).

Thermal Conductance of Phonon Waveguides in the Ballistic One-Dimensional Limit

In the limit of $kT << \hbar\omega_m$, only the four lowest modes contribute to the thermal conductance.

For ideal coupling ($T_m = 1$), a fundamental relation holds for each mode:

$$G_{th} = g_0 = \pi^2 k_B^2 T/(3h)$$

This quantum of thermal conductance represents the maximum possible value of energy transported per phonon mode.

K. Schwab, *et al.*, *Nature*, **404**, 974 (2000).

Comparing Electrical and Thermal Conductance Quantization

Quantum of electrical conductance is:

$$g_0 = 2e^2/h$$

Quantum thermal conductance is proportional to T since energy is being transported as opposed to quantum electrical conductance where charge is being transported.

K. Schwab, *et al.*, *Nature*, **404**, 974 (2000).

Comparing Electrical and Thermal Conductance Quantization

Electrical experiments lead to steps in the conductance that are not observed in thermal experiments.

In electrical experiments, the chemical potential and temperature can be independently varied. Consequently, at low temperature, the sharp edge of the Fermi-Dirac distribution function can be swept through 1-D modes.

With phonons, only the temperature can be swept. The broader Bose-Einstein distribution function smears out all features except the lowest lying modes at low temperature.

K. Schwab, *et al.*, *Nature*, **404**, 974 (2000).

Measurement of the Quantum Limit of Thermal Conductance

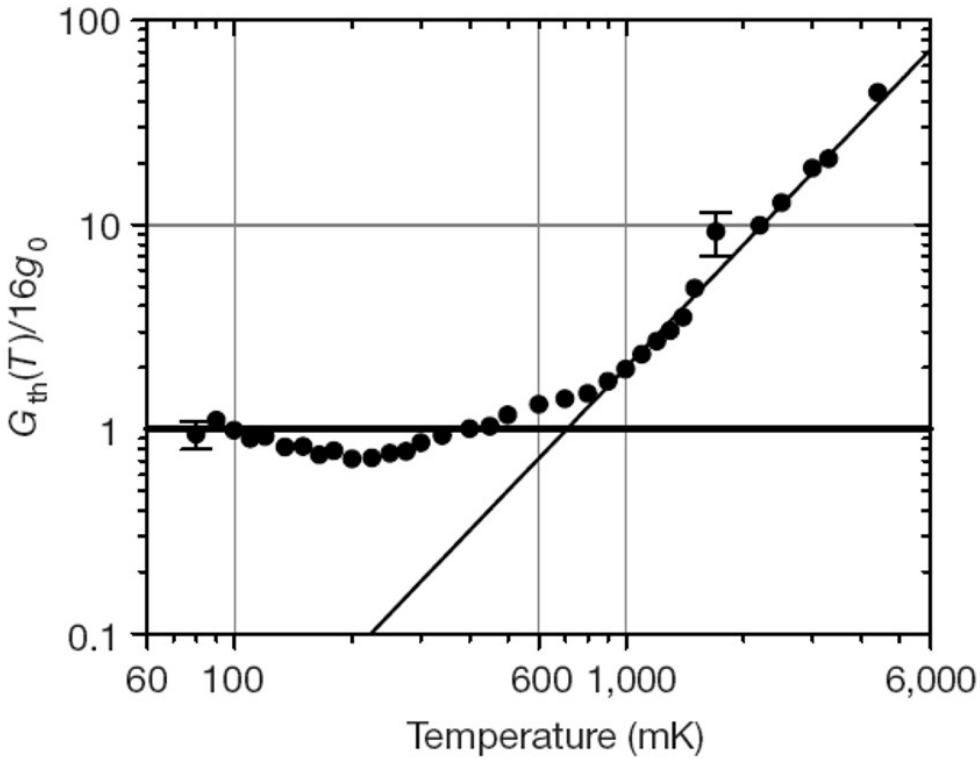

K. Schwab, *et al.*, *Nature*, **404**, 974 (2000).